Preparation of LiFePO₄ using iron(II) sulfate as product from titanium dioxide slag purification process and its electrochemical properties

Ju Guo[1,], Yulong Feng[1] , Xinliang Mo[1] , Gaojian Liao[2]*

[1] Moutai Institute, Renhuai 564507, Guizhou, China
[2] Wengfu (Group) Co., Ltd., Guiyang 550025, Guizhou, China
[*]E-mail: 158383434@qq.com

To further reduce the production cost of LiFePO₄ cathode material and promote the resource utilization of titanium dioxide slag solid waste, this paper chose titanium dioxide slag rich in iron(II) sulfate as raw material. After purification, it prepared LiFePO₄ and studied the differences in composition, structure, morphology and electrochemical properties of LiFePO₄ prepared from a commercially available battery-grade iron(II) sulfate as a comparison sample. The results showed that the purity of iron(II) sulfate in the purified titanium dioxide slag could reach 99.97% by using a composite precipitant formulated with ammonium bifluoride and reduced iron powder. LiFePO₄ prepared from it has an olivine structure with a micron-sized short rod shape. The first charge/discharge specific capacities were 161.55 and 159.33 mAh/g at 0.1C multiplie respectively. The coulomb efficiency reached 98.63%. After 200 cycles of charge/discharge at 1C multiplier, the capacity retention was still 95.05%, which was similar to the electrochemical performance of LiFePO₄ prepared from battery-grade iron(II) sulfate. The results of this paper indicate that the preparation of LiFePO₄ from titanium dioxide slag purification has good prospects for industrial application and may become a new way to solve the problem of solid waste utilization of titanium dioxide slag.

Keywords: titanium dioxide slag, iron(II) sulfate, LiFePO₄, performance

1. INTRODUCTION

Titanium dioxide slag is defined in the industry as a solid waste byproduct of titanium dioxide production by the sulfuric acid process. Its main component is iron(II) sulfate salt containing a certain amount of crystalline water and containing more magnesium, titanium and other metal impurity ions [1-2]. Because of its high impurity content, poor stability, and low economic value, titanium dioxide slag is difficult to be resourcefully utilized. It is mostly disposed of by pile storage, which causes

serious safety and environmental hazards [3-4]. Recent studies found that the high-purity iron(II) sulfate obtained from the purification of titanium dioxide slag can be used as the raw material of iron source required for the production of LiFePO$_4$ for lithium battery cathode materials. It has the advantages of low raw material prices and wide sources [5-7]. Therefore, the preparation of LiFePO$_4$ from titanium dioxide slag purification technology has gradually become a research hotspot.

At present, domestic and foreign titanium dioxide slag purification technology mainly includes crystallization method [8-9], precipitation method [10-11], and adsorption method [12-13], among which precipitation method is widely used because of low processing cost, short process flow, and convenient operation. For example, Peng [14] et al. used a single iron powder as a precipitant and used the precipitation method at a reaction temperature of 95 °C. The reaction time of this research is 6 hours. Hydrolyzing the titanium impurity ions in titanium dioxide slag into metatitanic acid precipitate and filtering it out, and then prepared and obtained high purity ferrous oxalate. Ruan [15] et al. used sodium sulfide as a precipitant to make the metal impurity ions in the aqueous solution of titanium dioxide, which produces sulfide precipitation and thus filtered and removed to obtain high-purity iron(II) sulfate. Existing studies have shown that the purity of iron(II) sulfate has an important influence on the electrochemical properties of synthesized LiFePO$_4$ [16-18]. The key factor in the purification of titanium dioxide slag by precipitation to obtain high purity iron(II) sulfate is the choice of precipitant. The traditional single-component precipitant is less effective in the face of multiple impurity ions. It still need to be supplemented by other post-treatment processes, which increases the complexity of the process [19-21]. To solve this problem, we intend to use a composite precipitant prepared by ammonium bicarbonate fluoride and iron powder in a certain mass ratio to remove impurities from titanium dioxide slag by a one-step precipitation method under certain reaction conditions. Choosing synthesize LiFePO$_4$ from the purified titanium dioxide slag and commercially available battery-grade iron(II) sulfate as raw material respectively, finding new ways for the resource utilization of titanium dioxide slag by comparing the performance of LiFePO$_4$ and thus judging its industrial application prospects.

The main research content of this paper includes: a titanium dioxide slag by-products were used as raw material. Ammonium fluoride and iron powder in a certain mass ratio of the composite precipitant was used to replace the traditional single chemical precipitant. A one-step precipitation method was used to remove Ti, Mg and other metal impurities in titanium dioxide slag and obtain high-purity iron(II) sulfate products and used as raw material to further prepare LiFePO$_4$. At the same time, a battery-grade iron(II) sulfate product from a commercially available was used to prepare LiFePO$_4$ as a comparison sample to study the performance difference between the two materials and to judge the industrialization prospect of LiFePO$_4$ prepared by titanium dioxide slag purification.

2. EXPERIMENTAL

2.1 Raw materials and equipment

Raw materials: titanium dioxide slag, iron(II) sulfate (battery grade), reduced iron powder, ammonium bifluoride, phosphoric acid, ammonia, lithium carbonate, glucose, etc.

Apparatus: polytetrafluoro hydrothermal reactor (2L), tube furnace, circulating water vacuum pump, electric blast dryer, and muffle furnace, etc.

2.2 Experimental methods

Titanium dioxide slag purification: A titanium dioxide slag was used as raw material (recorded as **TDS** for subsequent testing and analysis). The composite precipitant prepared by ammonium bicarbonate fluoride and reduced iron powder according to the mass ratio of 3.6:1 was selected. The one-step precipitation method was used to purify and remove impurities. The reaction conditions were controlled as follows: reaction temperature of 60 ℃, reaction time of 2 h, precipitant dosage of 2.67% (mass fraction) of the amount of titanium dioxide treated, Fe^{2+} concentration of 1.37 mol/L in the reaction solution, stirring speed of 300 rpm, and purification of high-purity iron(II) sulfate, which were recorded as **FS-T** for subsequent testing and analysis. A commercially available battery-grade iron(II) sulfate was used as a comparison sample and was recorded as **FS-B**. A sketch of the titanium dioxide slag purification process is shown in Figure 1a.

Preparation of $LiFePO_4$: The 30% phosphoric acid solution and 4% FS-T or FS-B solution were added to the reaction kettle at a substance ratio of 1.05:1. 1.1 times the theoretical amount of hydrogen peroxide was added. Ammonia was added as a pH adjuster in the right amount. During the reaction process, the reaction temperature was controlled at 50 °C. The pH of the reaction solution was 3. The reaction time was 6 h. When the reaction finished, the reaction solution was filtered and washed. The filter cake was dried at 120 °C. Then it was mixed with lithium carbonate and glucose, calcined at 750 °C for 8 h in a nitrogen atmosphere, cooled and ground to prepare $LiFePO_4$. The ratio of lithium carbonate to iron phosphate substance added was 0.52:1. The amount of glucose added was 10% of the mass of iron phosphate. The $LiFePO_4$ prepared from FS-T was noted as **LFP-T** for subsequent analysis. The $LiFePO_4$ prepared from FS-B was noted as **LFP-B**. A sketch of the $LiFePO_4$ preparation process is shown in Figure 1b.
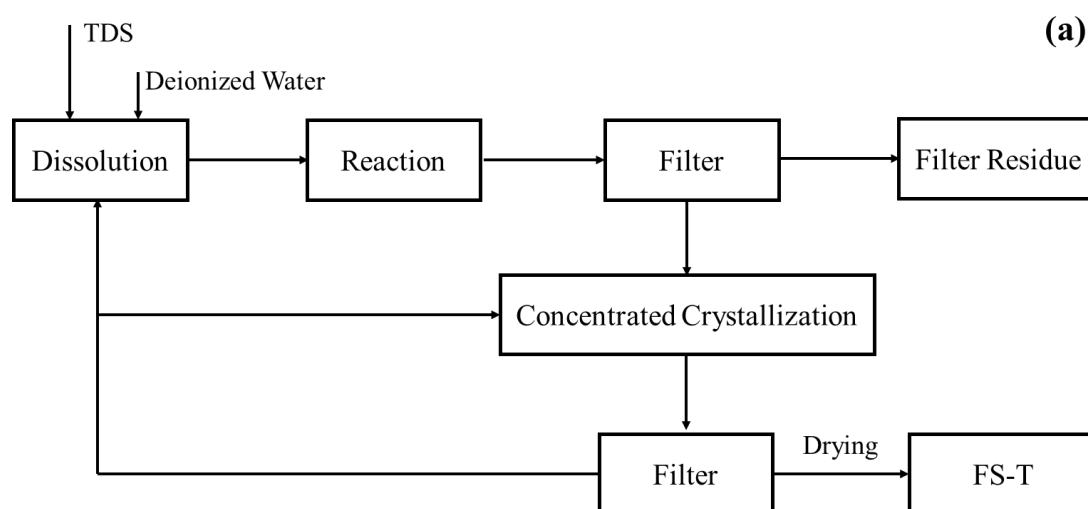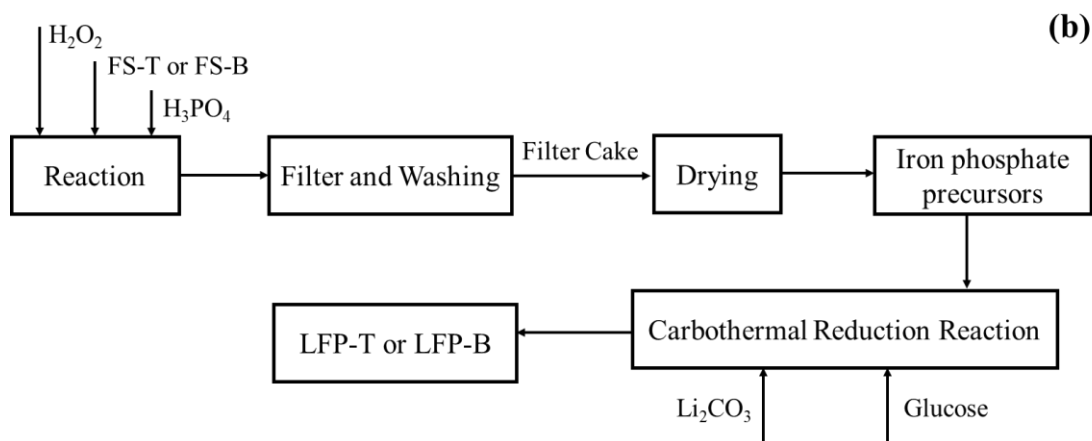
Figure 1. Schematic diagram of the experimental scheme, (a) titanium dioxide slag purification process flow chart; (b) LiFePO$_4$ preparation process Flowchart

2.3 Characterization

ICP-OES (PE Optima 7000, USA) was used to analyze the elemental composition content of the samples. XRD (X'Pert Powder III, Panaco, the Netherlands) and XPS were used to characterize the sample structure. SEM (Zeiss SIGMA-500, Germany) was used to characterize the sample morphology. A laser particle size analyzer (Malvern Mastersizer 3000) was used to analyze the particle size of the samples.

The Wuhan Blue Battery Test System (LAND-BT2013A) was used for constant current charge/discharge and cycling performance tests at different multipliers at room temperature, with a voltage range of 2.0-4.2 V and charge/discharge multipliers of 0.1C, 1C, 2C and 5C. The LiFePO$_4$ batteries were prepared as follows: LFP-T and LFP-B were prepared as the cathode active substance. Acetylene black were prepared as the conductive agent. Polyvinylidene fluoride were prepared as the adhesive respectively. According to the mass ratio of 75:15:10, N-methyl-2-pyrrolidone was prepared as the solvent to make a slurry coated on aluminum foil. Putting it into Vacuum drying at 120 ℃ for 12 h and then made it into a disc as the positive electrode sheet. The lithium sheet was used as the negative electrode. 1 mol/L LiPF$_6$ solution of vinyl carbonate/dimethyl carbonate (1:1 by volume) was used as the electrolyte. Polypropylene microporous membrane was used as the diaphragm of the battery, which was assembled into CR2032 button cell in the glove box. Each button cell contained 150 mg of active substance.

3. RESULTS AND DISCUSSION

In order to study the effect of purification and decontamination of titanium dioxide slag, the unpurified titanium dioxide slag (TDS), purified titanium dioxide slag (FS-T), and a commercially available battery-grade iron(II) sulfate (FS-B) were taken as samples for component content analysis. The results obtained are shown in Table 1.

Table 1. Composition of iron(II) sulfate before and after purification of titanium dioxide slag and a commercially available battery grade

Sample	Purity (FeSO$_4$·7H$_2$O)	Mg	Ti	Ca	Mn	Ni	Na
TDS（%）	91.28	0.76	0.077	0.003	0.0095	0.001	0.0015
FS-T（%）	99.97	0.0036	0.0001	0.009	0.0042	-	0.0007
FS-B（%）	99.94	0.009	0.0003	0.026	0.0027	0.001	0.0008

"-" indicates no detection.

It can be seen from the data in Table 1 that the main component of TDS is FeSO$_4$·7H$_2$O whose content is 91.28%. The impurity content is mainly metal ions, such as Mg and Ti, reaching 0.76% and 0.077% respectively. The remaining impurity content, such as Ca, Mn, Ni, and Na are low, all below 100 ppm. The remaining amount is free water. It can be seen that the goal of TDS purification and impurity removal is mainly to remove the metal impurity ions, such as Mg and Ti. The purity of FS-T was significantly improved by adding the compound precipitant described in this paper, reaching 99.97%. This is comparable to the content of FS-B. At the same time, a significant reduction of impurities, for example, Mg and Ti was observed, where the Mg content was reduced to 0.0036% with 99.53% removal and Ti content was reduced to 0.0036% with 99.87% removal. The remaining trace impurity elements were also removed to some extent. Comparing the results of FS-T and FS-B composition, it can be seen that the method described in this paper has achieved excellent purification and decontamination results. The composition of FS-T after decontamination is similar to that of commercially available battery grade FS-B.

The process of one-step precipitation purification of titanium dioxide slag using a composite precipitant consists of four main steps [22]. Firstly, the reduced iron powder contained in the composite precipitant reacts with the excess sulfuric acid in the titanium dioxide solution to reduce the acidity of the solution. Secondly, the excess reducing iron powder reduces the Fe^{3+} formed after oxidation of the titanium dioxide slag to Fe^{2+}. Then, under neutral and weakly acidic conditions, the TiO^{2+} in titanium dioxide slag undergoes hydrolysis to generate H$_2$TiO$_3$ precipitate and thus is removed by filtration, reducing the Ti content. Finally, the ammonium hydrogen fluoride in the compound precipitant ionizes F$^-$ and precipitates with Mg^{2+} in the titanium dioxide slag to form MgF$_2$ precipitate to be filtered and removed, reducing the Mg content. The main reaction equations are:

（1）Fe＋2H$^+$→Fe^{2+}＋H$_2$↑

（2）Fe^{3+}＋Fe→2Fe^{2+}

（3）TiO^{2+}＋2H$_2$O→H$_2$TiO$_3$↓＋2H$^+$

（4）Mg^{2+}＋2F$^-$→MgF$_2$↓
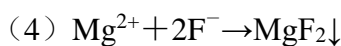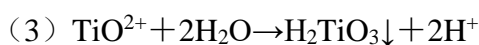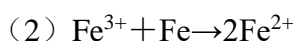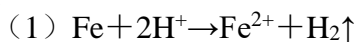
Further, FS-T was used as raw material to prepare LiFePO$_4$ cathode material which recorded as LFP-T according to the experimental method described in subsection 2.2, and LiFePO$_4$ prepared by

FS-B with the same method which recorded as LFP-B as a comparison sample to analyze the differences in the composition of the two samples. The results obtained are shown in Table 2.

Table 2 Composition of LFP-T and LFP-B

	Li（%）	Fe（%）	P（%）	Mg（%）	Ti（%）
LFP-T	4.52	35.37	19.66	0.0002	-
LFP-B	4.55	35.29	19.73	0.0004	-

"-" indicates no detection.

As can be seen from the data in Table 2, the composition of LFP-T and LFP-B samples are basically the same. The main element contents Li, Fe, P, etc. are relatively close, 4.52%, 4.55%, 35.37%, 35.29%, 19.66%, and 19.73%, respectively. The main impurity content Mg, Ti further reduced. All of them meet the requirements of China's national standard GB/T 30835-2014 for LiFePO$_4$ for batteries. This indicates that the preparation of LiFePO$_4$ for lithium batteries after purification of titanium dioxide solid waste is feasible. It is basically consistent with LiFePO$_4$ prepared from a commercially available battery-grade iron(II) sulfate in terms of product composition.

The process of preparing LiFePO$_4$ cathode materials from FS-T or FS-B is divided into two main stages [23-24]. The first stage is the preparation of iron phosphate precursors by liquid-phase precipitation, with the main reaction equation: $2FeSO_4 + H_2O_2 + H_2SO_4 = Fe_2(SO_4)_3 + 2H_2O$, $Fe_2(SO_4)_3 + 2H_3PO_4 + 6NH_4OH = 2FePO_4\downarrow + 3(NH_4)_2SO_4 + 6H_2O$. The second stage is the preparation of LiFePO$_4$ cathode material by carbon thermal reduction method. The main reaction equation is $2FePO_4 + Li_2CO_3 + C = 2LiFePO_4 + CO_2\uparrow + CO\uparrow$.

In the preparation stage of iron phosphate precursor system, there are two stages of nucleation and growth while the liquid phase precipitation reaction occurs. Therefore, the impurity ion content of the reaction materials FS-T and FS-B are critical. If the impurity ion content is too high, this will lead to ion packing and high impurity content of the synthesized iron phosphate precursors. In the second stage of LiFePO$_4$ synthesis by carbon thermal reduction, the precursor metal impurity ions will further affect the purity of the prepared LiFePO$_4$ product, thus affecting the electrochemical properties of the material. Combining the data in Tables 1 and 2, it can be seen that a better impurity removal effect was obtained by using the titanium dioxide slag purification technique described in this paper, which resulted in high purity and basically uniform composition of the prepared LFP-T and LFP-B samples.

Figure 2 shows the XRD and XPS test results of samples, where Figure 2a shows the XRD spectra of FS-T and FS-B samples. Figure 2b shows the XRD spectra of LFP-T and LFP-B. Figure 2c and d show the XPS total and Fe fraction spectra of LFP-T and LFP-B samples, respectively. As shown in Fig. 2a, the characteristic diffraction peaks of FS-T and FS-B were basically consistent and matched with the standard material card of JPDS01-072-1106, indicating that the samples are iron(II) sulfate heptahydrate, which indicated that high purity iron(II) sulfate heptahydrate was obtained from titanium dioxide slag after purification and impurity removal. It was also consistent with the results of sample composition content obtained in Table 1. Figure 2b shows the XRD spectra of LFP-T and LFP-

B. As it can be seen from the figure, the characteristic XRD diffraction peaks of the two samples are relatively sharp and consistent with the JPDS01-077-0179 spectrum, indicating that the samples are $LiFePO_4$ with olivine structure and high crystallinity. No diffraction peaks of other substances were observed from the spectra, indicating the high purity of the samples. The reason is that the use of high-purity FS-T and FS-B samples were prepared as raw materials, indicating that a good decontamination effect was achieved by using the purification process described in this paper. To further characterize the composition and structure of LFP-T and LFP-B samples, they were analyzed by XPS. The results are shown in Figure 2c and d. Figure 2c shows that both LFP-T and LFP-B samples are composed of Li, Fe, P, and O elements. The corresponding energy spectrum peaks are at 54.69, 712.65, 133.84, and 531.7 ev, respectively [25]. Also, the energy spectrum peak characterizing C was observed at 284.8 eV, which is due to the thermal decomposition of excess glucose added during the thermal reduction [26]. Figure 2d shows the Fe spectra obtained by further peak splitting of elemental Fe using Avantage software. The results show that the Fe elements of both samples are all Fe^{2+} peaks [27], and no energy spectrum peaks characterizing Fe^{3+} were observed. It is also evident from Figure 2d that the Fe fraction peaks of LFP-T prepared from titanium dioxide slag purification and LFP-B prepared from battery-grade iron(II) sulfate remain consistent, which indicates that all Fe^{3+} of the iron phosphate precursors were reduced to Fe^{2+}.
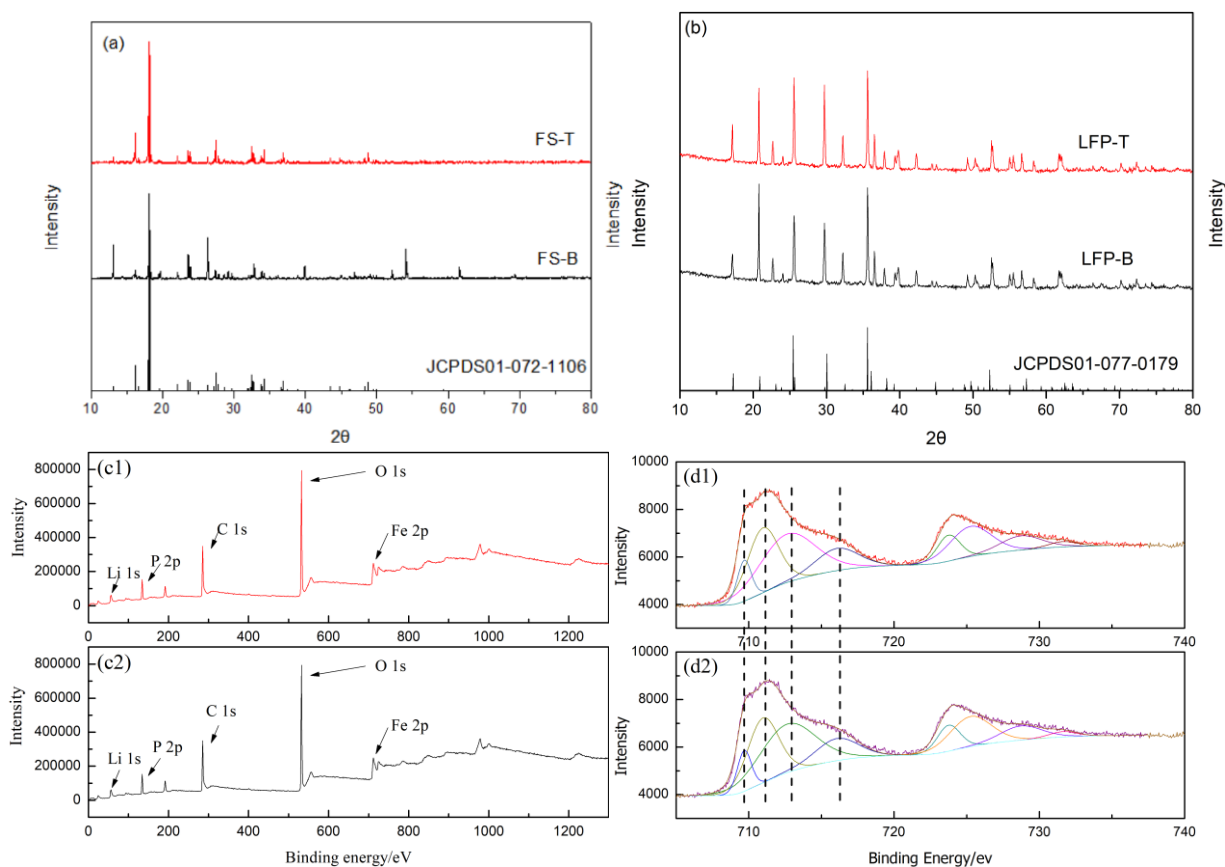

Figure 2. XRD (a, b) and XPS (c, d) spectra of the samples, (a) FS-T, FS-B; (b) LFP-T, LFP-B; (c) LFP-T, LFP-B total spectrum. (d) LFP-T, LFP-B subspectra

Figure 3 shows the SEM images of the sample, where Figure 3a shows the FS-T morphology, Figure 3b shows the FS-B morphology, Figure 3c shows the LFP-T morphology, Figure 3d shows the LFP-B morphology. The accompanying figure shows its local enlargement image. From Fig. 3a, it can be seen that the FS-T sample obtained after the purification of titanium dioxide slag is in the shape of micron-level short rods with the particle size of about 10-20 μm and obvious grain boundaries. However, the FS-B sample shown in Fig. 3b is in the shape of micron-level disordered particles with a slightly smaller particle size than the FS-T sample, about 5-10 μm. Besides, it has a slight agglomeration phenomenon, because the fact that the FS-T sample was obtained by concentrating and crystallizing the titanium dioxide slag after purification. The supersaturation of the concentrated filtrate gradually increased during the process of gradual cooling. The FS-T nuclei gradually precipitated from the solution and grew with time, growing into crystals with short rod-like morphology and significant grain boundaries under the influence of crystal plane potential energy. The purchased FS-B sample is a commodity produced by subsequent crushing and other processes. Therefore, its particle size is lower than that of the FS-T sample. The crushed FS-B sample has a larger surface energy, which causes a certain degree of particle agglomeration phenomenon. Figure 3c and Figure 3d show the microscopic morphology pictures of LFP-T and LFP-B samples prepared from FS-T and FS-B, respectively. As it can be seen from the figures, the morphologies of both LFP-T and LFP-B samples retain some of the morphological features of their precursors, with a certain degree of particle size reduction because of the fact that in the preparation of $LiFePO_4$ by carbothermal reduction. The iron phosphate precursor, as a reaction substrate at 750 °C, reacts with the molten lithium carbonate that penetrates into the precursor under the reducing atmosphere formed by glucose decomposition [28]. Therefore, the precursor morphology has an induced effect on the product morphology, which is slightly reduced by the effect of lithium carbonate thermal decomposition during the reaction. It is further evidenced by the particle size distribution data (Table 3 and Fig. 3e, f). Figure 3e and f show the particle size distribution of FS-T, FS-B, LFP-T, and LFP-B, respectively. Table 3 shows their corresponding particle size data. It can be seen that the median particle size of FS-T obtained after titanium dioxide slag purification is about 15.6 μm. The median particle size of synthesized LFP-T is reduced to 2.5 μm. The median particle size of the commercially available battery grade FS-B sample was 5.7 μm. The median particle size of the synthesized LFP-B was 3.2 μm.
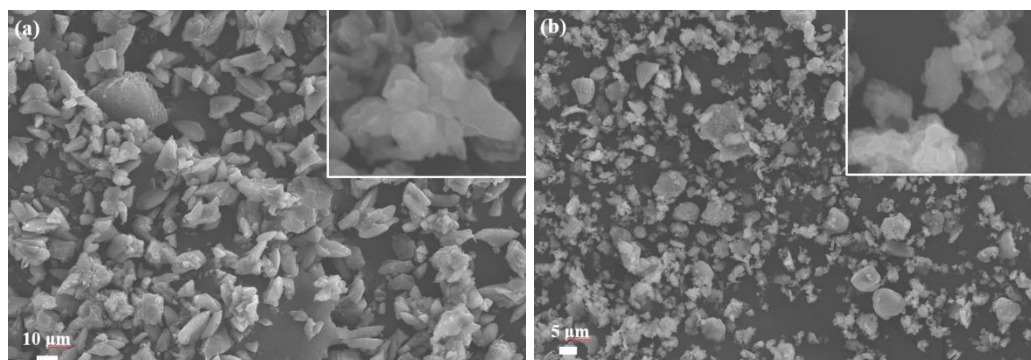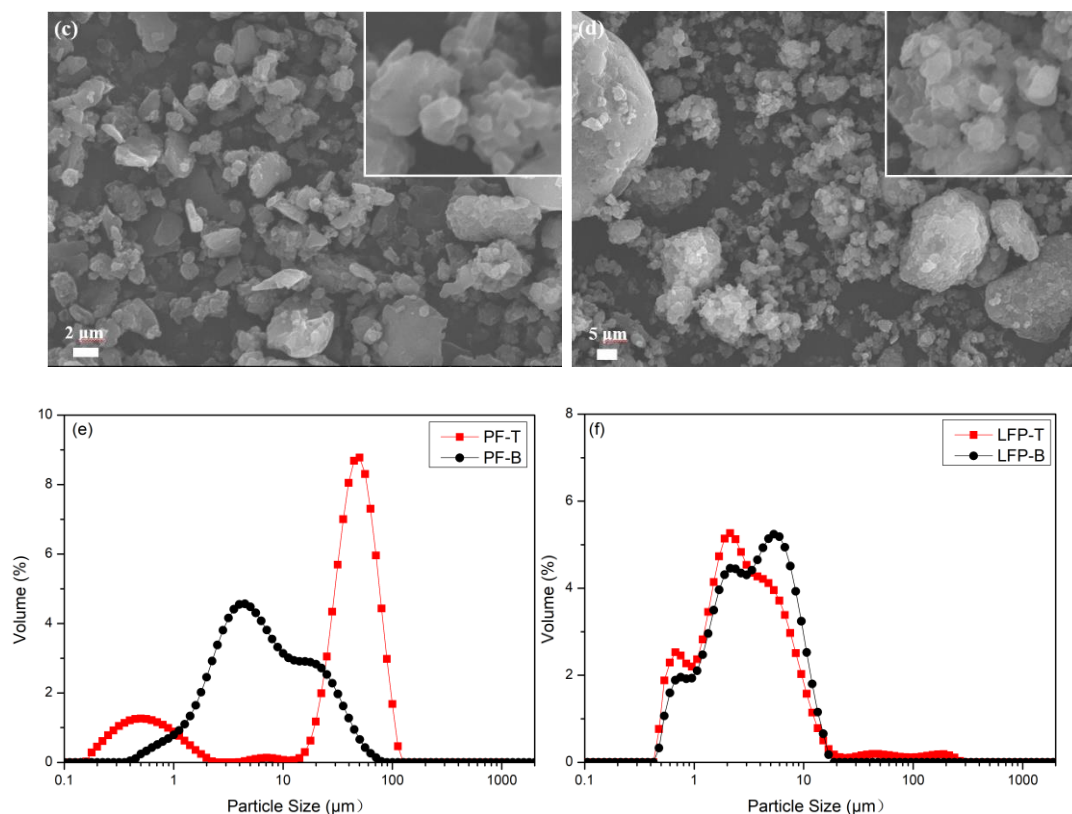
Figure 3. SEM (a, b, c, d) and Size (e, f) images of the samples, (a) FS-T; (b) FS-B; (c) LFP-T; (d) LFP-B; (e) FS-T and FS-B; (f) LFP-T and LFP-B.

Table 3. Particle sizes of FS-T, FS-B, LFP-T, and LFP-B samples

	D_{10} (µm)	D_{50} (µm)	D_{90} (µm)
FS-T	1.1	15.6	28
FS-B	1.7	5.7	24.1
LFP-T	0.8	2.5	8.4
LFP-B	0.9	3.2	14.4

Figure 4 shows the electrochemical performance test results of the LFP-T and LFP-B samples, where Figure 4a shows the first charge/discharge performance curves of the LFP-T and LFP-B samples at 0.1C magnification. Figure 4b shows the first charge/discharge performance curves of LFP-T and LFP-B samples at 5C magnification. Figure 4c shows the performance curves of LFP-T and LFP-B samples at 0.1C, 1C, 2C, and 5C multipliers, respectively. Figure 4d shows the cycling performance of LFP-T and LFP-B samples at 1C multiplier for 200 cycles. From Figure 4a, it can be seen that under 0.1C multiplicity conditions, both LFP-T and LFP-B have stable charge and discharge voltage plateaus near about 3.4 V with a small difference of about 0.9 V. This indicates that the polarization of the materials is small during the discharge process and that the materials have good reversible and stable performance [29]. From Figure 4a, it can also be seen that the first

charge/discharge specific capacities of the LFP-T and LFP-B samples were 161.55, 159.33 mAh/g and 161.96, 159.92 mAh/g, respectively. at 0.1C magnification, with coulomb efficiencies of 98.63% and 98.74%, respectively. This indicates that the first charge/discharge performance of LFP-T prepared from FS-T purified from titanium dioxide slag and LFP-B material prepared from commercially available battery-grade FS-B are similar at low multiplicity conditions (0.1C) with comparable coulomb efficiencies. While the results of the first charge/discharge curves at high magnification conditions (5C), it shows (Figure 4b) that both LFP-T and LFP-B still have a stable charge/discharge voltage plateau around 3.4V. However, their difference values increased to 0.23 V and 0.21 V, respectively. Their first charge/discharge specific capacities reached 118.14, 110.62 mAh/g, 118.86, and 111.71 mAh/g, respectively, with coulomb efficiencies of 93.63% and 93.98%, respectively. Although the first charge/discharge specific capacities and coulomb efficiencies of LFP-T and LFP-B at 5C magnification decreased compared with those at 0.1C magnification, the differences between LFP-T and LFP-B samples were not significant. Combining the data in Figs. 4a and 4b, it can be seen that LFP-T exhibited similar first charge/discharge performance as LFP-B both at low magnification (0.1C) and at high magnification conditions (5C). This indicates that the $LiFePO_4$ prepared from titanium dioxide slag purification has similar electrochemical performance to that of $LiFePO_4$ from battery-grade iron(II) sulfate, i.e., the $LiFePO_4$ prepared from titanium dioxide slag purification has good prospects for industrial application. This conclusion is further supported by the results of multiplicative and cycling performance tests of the samples.

Figure 4c shows the multiplicity performance curves of LFP-T and LFP-B samples. The first discharge specific capacities of LFP-T and LFP-B were 159.11 and 159.75 mAh/g, respectively. When they started to discharge at 0.1C after 1C, 2C, and 5C multiplicity conditions and then returned to 0.1C again, and the irreversible specific capacities were only 0.19 and 0.17 mAh/g, compared with their initial values, respectively. This indicates that the discharge specific capacities of LFP-T and LFP-B materials are less affected after a large multiplicative current shock. The discharge specific capacities can be almost fully recovered [30], which also proves that both LFP-T and LFP-B have good multiplicative performance. The first discharge specific capacities of LFP-T were measured to be 159.3, 146.74, 134.6, and 110.6 mAh/g at 0.1C, 1C, 2C, and 5C multiplicity conditions, respectively. The first discharge specific capacities of LFP-B under 0.1C, 1C, 2C and 5C multiplicity conditions were 159.92, 147.6, 135.51, and 111.71 mAh/g, respectively. The above results indicated that the multiplicity performance of LFP-T and LFP-B were comparable. Figure 4d shows the discharge specific capacities of LFP-T and LFP-B samples cycled 200 times under 1C multiplicity condition, and their discharge specific capacities after the initial and 200 cycles were 146.74, 139.47 mAh/g, 147.56 , and 141.09 mAh/g, respectively. The capacity decay rates were 95.05% and 95.62%, respectively, indicating that the two kinds have similar cycling performance.
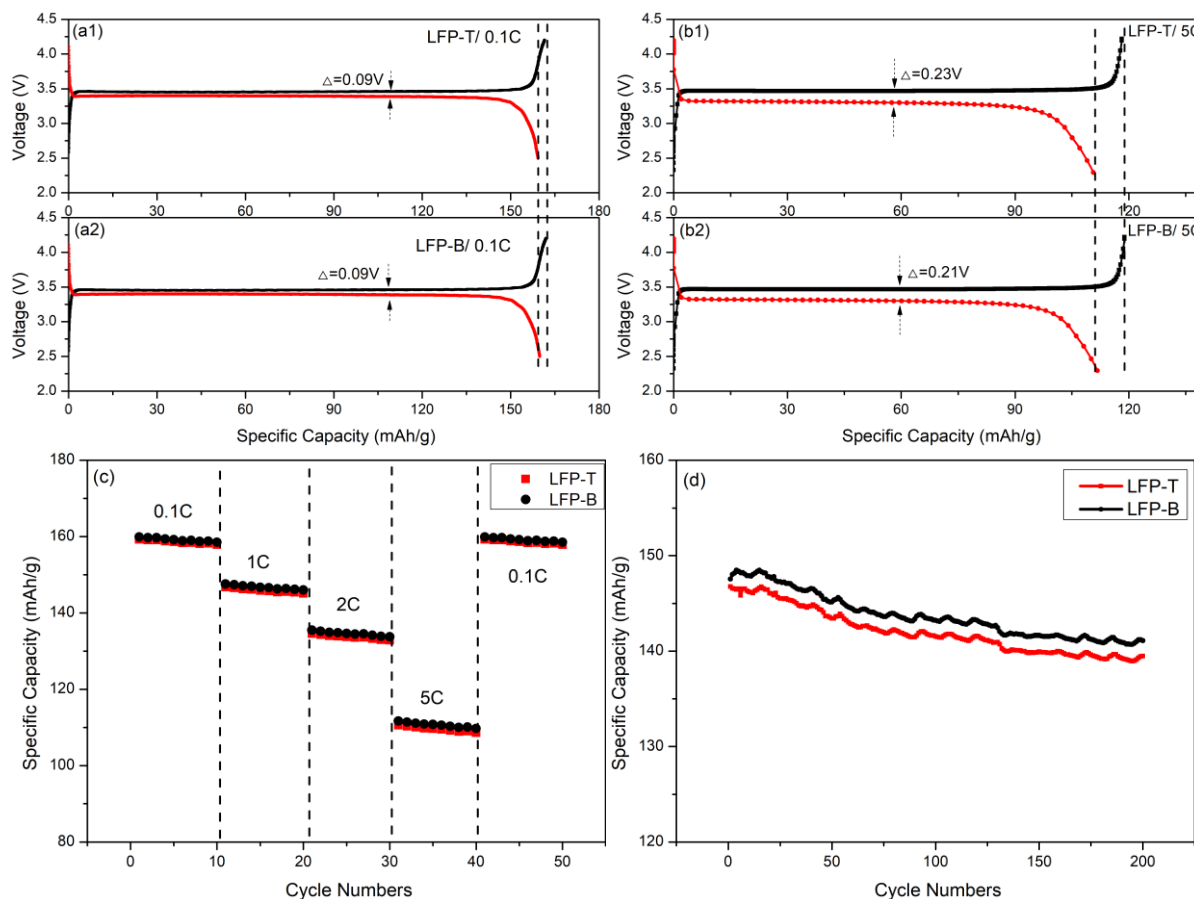
Figure 4. Electrochemical performance of the samples, (a) first charge/discharge performance at 0.1C; (b) first charge/discharge performance at 5C; (c) multiplier performance; (d) cycling performance

In order to further analyze the industrial feasibility and potential advantages of purifying titanium dioxide slag to prepare $LiFePO_4$, we compared the electrochemical properties of LFP-T prepared with FS-T obtained by the purification technology described in this paper with similar cathode materials described in relevant literature in recent years. The results are shown in Table 4. It can be seen from the data in Table 4 that the first discharge specific capacity of LFP-T reaches 159.3 mAh/g at 0.1C and 110.6 mAh/g at 5C, which are better than those cathode materials recorded in references listed in table 4. It shows that iron(II) sulfate with high purity is successfully prepared by one-step precipitation method with the addition of composite precision prepared in a certain mass ratio of ammonium fluoride and iron powder which is conducive to improve the electrochemical performance of $LiFePO_4$, and also exhibits that the purification of titanium dioxide slag to prepare $LiFePO_4$ has a good industrial prospect.

Table 4. Comparison of electrochemical properties of materials

Ref	Initial discharge capacity （mAh/g）
This work	159.3 (0.1C); 146.7 (1C); 134.6 (2C); 110.6 (5C)
[6]	152 (1C); 142 (2C); 126 (5C)
[9]	161 (0.1C); 145 (1C); 134 (2C); 112(5C)
[23]	152 (0.1C); 129(1C)
[27]	136.4 (0.1C); 109.9 (1C)
[30]	150 (0.1C); 135 (0.5C); 110 (1C); 90 (5C)

4. CONCLUSIONS

High-purity iron(II) sulfate was prepared by using a titanium dioxide slag solid waste as raw material, using a composite precipitant combined with a one-step precipitation method to purify and remove impurities such as Mg and Ti ions. The removal rate reached 99.53% and 99.87%, respectively. The purity of the obtained iron(II) sulfate reached 99.97%. Then, $LiFePO_4$ cathode materials were further synthesized from the purified titanium dioxide slag. $LiFePO_4$ synthesized using a commercially available battery-grade iron(II) sulfate was used as a comparison sample. The results show that the two materials have the same structure and similar composition, while the morphology is influenced by their precursors. The electrochemical performance test results show that the specific capacity of discharge at 0.1C or 5C multiplier conditions are relatively close, indicating that the preparation of $LiFePO_4$ from titanium dioxide slag purification is feasible and has good prospects for industrial application. It may become a new way to solve the problem of solid waste utilization of titanium dioxide slag.

CONFLICTS OF INTEREST
There are no conflicts to declare.

References

1. A. He, G. Chen, J. Chen, J.H. Peng, C. Srinivasakannan and R.S. Ruan, *Powder Technol.*, 323 (2018) 115.
2. F.Q. Zheng, Y.F. Guo, S.S. Liu, G.Z. Qiu, F. Chen, T. Jiang and S. Wang, *Trans. Nonferrous Met. Soc. China*, 28 (2018) 356.
3. G.K. Ren, X.L. Wang, Z.Y. Zhang, B.H. Zhong, L. Yang and X.S. Yang, *Dyes Pigm.*, 147 (2017) 24.
4. W. Lv, X.W. Lv, J.Y. Xiang, Y.Y. Zhang, S.P. Li, C.G. Bai, B. Song and K.X. Han, *Int. J. Miner. Process.*, 167 (2017) 68.
5. J.L. Li, J.H. Wu, Y. Li, H. Zhao, T.L. Zhao, S.Q. Ma and H. Liu, *J. Taiwan Inst. Chem. Eng.*, 99 (2019) 74.
6. L. Wu, Z.X. Wang, X.H. Li, H.J. Guo, L.J. Li, X.J. Wang and J.C. Zheng, *J. Alloys Compd.*, 497 (2010) 278.

7.   J. Guo, J.X. Cao and S.Z. Jia, *Int. J. Electrochem. Sci.,* 15 (2020) 10524.
8.   W.L. Nie, S.M. Wen, Q.C. Feng, D. Liu and Y.W. Zhou, *J. Mater. Res. Technol.*, 28 (2019) 1750.
9.   L. Wu, X.H. Li, Z.X. Wang, L.J. Li, J.C. Zheng, H.J. Guo, Q.Y. Hu and J. Fang, *J. Power Sources*, 189 (2009) 681.
10. Q.Y. Lei, D.W. He, K.G. Zhou, X.K. Zhang, C.H. Peng and W. Chen, *J. Rare Earths*, 07 (2020) 1.
11. W. Purcell, M.K. Sinh, A.Q. Vilakazia and M.N. Selective, *Hydrometallurgy*, 191 (2020) 105242.
12. Z.Z. Bian, Y.L. Feng and H.R. Li, *Trans. Nonferrous Met. Soc. China*, 30 (2020) 2826.
13. S. Middlemas, Z.Z. Fang and P. Fan, *Hydrometallurgy*, 131 (2013) 107.
14. A.G. Peng, Z.C. He, C.Y. Yu, W. Xiao, X.J. Zhuang and Y. Liu, *Inorganic Chemicals Industry*, 44 (2012) 60. (In Chinese)
15. H. Ruan, J.H. Yi and F.Z. Gong, *Technology & Development of chemical industry*, 41 (2012) 10. (In Chinese)
16. F. Wang, F.F. Wang, R.Y. Hong, X.S. Lv, Y. Zheng and H.Y. Chen, *J. Mater. Res. Technol.*, 5 (2020) 10004.
17. N.N. Zhao, Y.S. Li, X.X. Zhao, X.K. Zhi and G.C. Liang, *J. Alloys Compd.*, 683 (2016) 123.
18. M. Chen, L.L. Shao, H.B. Yang, Q.Y. Zhao and Z.Y. Yuan, *Electrochim. Acta*, 168 (2015) 59.
19. Y.J. Xiong, T. Aldahri, W.Z. Liu, G.R. Chu, G.Q. Zhang, D.M. Luo, H.R. Yue, B. Liang and C. Li, *Chin. J. Chem. Eng.*, 28 (2020) 2256.
20. G. Chen, Q. Jiang, K.Q. Li, A. He, J.H. Peng, M. Omrand and J. Chen, *J. Hazard. Mater.*, 388 (2020) 122039.
21. F.Q. Zheng, Y.F. Guo, G.Z. Qiu, F. Chen, S. Wang, Y.L. Sui, T. Jiang and L.Z. Yang, *J. Hazard. Mater.*, 344 (2018) 490.
22. J. Guo. *Inorganic Chemicals Industry*, 51 (2019) 48. (In Chinese)
23. B.Q. Zhu, X.H. Li, Z.X. Wang and H.J. Guo, *Mater. Chem. Phys.*, 98 (2006) 373.
24. M. Davidson, C. Ngo, S.H. Gage, S. Pylypenko and B.G. Trewyn, *Microporous Mesoporous Mater.*, 276 (2019) 270.
25. L.Y. Zhang, Y.F. Tang, Z.Q. Liu, H.N. Huang, Y.Z. Fang and F.Q. Huang, *J. Alloys Compd.*, 627 (2015) 132.
26. Y.Q. Chen, K.X. Xiang and W. Zhou. *J. Alloys Compd.*, 749 (2018) 1063.
27. J. Xia, F.L. Zhu, G.R. Wang, L. Wang, Y.S. Meng and Y. Zhang, *Solid State Ionics*, 308 (2017) 133.
28. Z.X. Chi, W. Zhang and F.Q. Cheng, *RSC Adv.*, 4 (2014) 7795.
29. Y. Li, J. Wang, J. Yao, H.X. Huang, Z.Q. Du, H. Gu and Z.T. Wang, *Mater. Chem. Phys.*, 224 (2019) 293.
30. C.C. Yang, J.H. Jiang and J.R. Jiang, *Energy Procedia*, 61 (2014) 1402.